

Switching Protein Conformational Substates by Protonation and Mutation

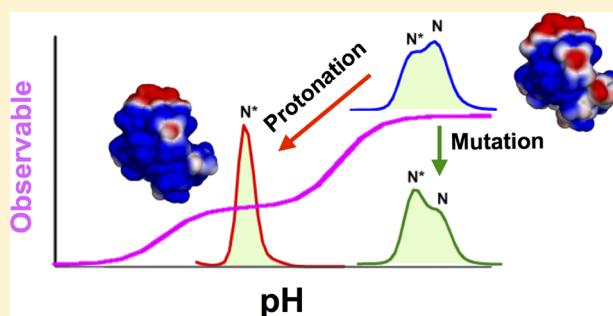
Abhishek Narayan¹ and Athi N. Naganathan^{1*}

Department of Biotechnology, Bhupat & Jyoti Mehta School of Biosciences, Indian Institute of Technology Madras, Chennai 600036, India

Supporting Information

ABSTRACT: Protein modules that regulate the availability and conformational status of transcription factors determine the rapidity, duration, and magnitude of cellular response to changing conditions. One such system is the single-gene product Cnu, a four-helix bundle transcription co-repressor, which acts as a molecular thermosensor regulating the expression of virulence genes in enterobacteriaceae through modulation of its native conformational ensemble. Cnu and related genes have also been implicated in pH-dependent expression of virulence genes. We hypothesize that protonation of a conserved buried histidine (H45) in Cnu promotes large electrostatic frustration, thus disturbing the H-NS, a transcription factor, binding face.

Spectroscopic and calorimetric methods reveal that H45 exhibits a suppressed pK_a of ~ 5.1 , the protonation of which switches the conformation to an alternate native ensemble in which the fourth helix is disordered. The population redistribution can also be achieved through a mutation H45V, which does not display any switching behavior at pH values greater than 4. The Wako–Saitô–Muñoz–Eaton (WSME) statistical mechanical model predicts specific differences in the conformations and fluctuations of the fourth and first helices of Cnu determining the observed pH response. We validate these predictions through fluorescence lifetime measurements of a sole tryptophan, highlighting the presence of both native and non-native interactions in the regions adjoining the binding face of Cnu. Our combined experimental–computational study thus shows that Cnu acts both as a thermo- and pH-sensor orchestrated via a subtle but quantifiable balance between the weak packing of a structural element and protonation of a buried histidine that promotes electrostatic frustration.



INTRODUCTION

The conformational flexibility of transcription factors (TFs) enables the rapid search of cognate binding sites on DNA. The availability and transcriptional fecundity of TFs, on the other hand, are determined by multiple variables, including the concentration of small molecules or ligands, proteins, oligomerization, allosteric switches, and environmental conditions.^{1–10} Certain protein modules can themselves up- or down-regulate the expression of specific genes. One such example in the enterobacteriaceae is the four-helix Hha-family of proteins that regulates the availability of the transcription factor H-NS.^{11–15} Mutational studies^{16,17} and spectroscopic experiments provide strong evidence that Cnu (YdgT), a member of the Hha-family, exhibits graded structural polymorphism with temperature¹⁸ that could be critical for the expression of virulence genes in enterobacteriaceae by modulating the binding affinity with H-NS.¹⁹

Apart from temperature, pH is another variable that undergoes dramatic changes as enterobacteriaceae invade a mammalian host and attempt to survive in the gastrointestinal tract. While diverse mechanisms exist to maintain pH-homeostasis,^{20–22} acidification of the cytoplasm could also act as a signal for successful invasion of the host. Interestingly,

the proteins Hha and Cnu have been implicated in the pH dependent expression of virulence factors in *Salmonella* pathogenicity island 2 (SPI-2).²³ This raises the question of whether Cnu senses pH to regulate the expression of virulence genes in a timely manner. What could the sensing mechanism involve? Studies on the effects of pH changes on the protein structure have a long history with protonation predominantly inducing unfolding of proteins at a low pH (<4), primarily due to the loss of favorable charge–charge interactions that counterbalance unfavorable electrostatics.^{24–27} At intermediate pH values ($4 < \text{pH} < 8$), mechanisms involve protonation coupled with conformational equilibria (or vice versa) between partially structured states, molten-globule like conformations and/or between folded and unfolded states.^{25–39} Structurally, such equilibria are generally governed by strategic location of histidines and other charged residues, such that the micro-environment contributes to perturbed pK_a values.

Special Issue: William A. Eaton Festschrift

Received: May 28, 2018

Revised: July 6, 2018

Published: July 26, 2018

In this regard, Cnu has three histidine residues, H25 (100% solvent exposed), H45 (60%), and H68 (100%), of which H45 is the most likely candidate given its partially buried nature (Figure 1A). Electrostatic potential calculations reveal that the

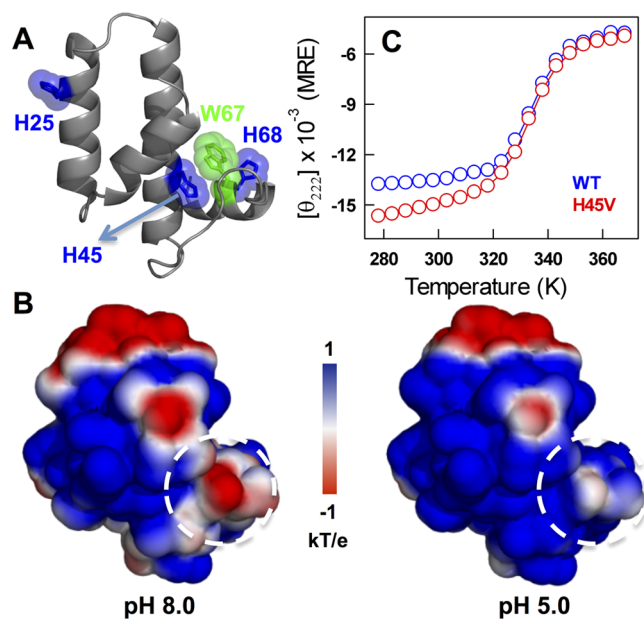


Figure 1. (A) Structure of Cnu indicating the location of the histidines (blue) and the lone tryptophan, W67. (B) Electrostatic potential map of Cnu at pH 8 (left) and pH 5 (right) in an identical orientation to the representation in panel A. It can be seen that the favorable potential around H45 (white circles in panel B) becomes more unfavorable on protonation. (C) Far-UV CD unfolding curves (in MRE units of deg·cm²·dmol⁻¹) of Cnu WT and the H45V mutant. Note the steeper pretransition in the mutant at temperatures less than 320 K.

neighborhood of deprotonated H45 has a favorable potential compared to when H45 is protonated (Figure 1B). We hypothesize that the protonation of H45 promotes large electrostatic frustration, driving conformational transition into partially structured states in the native ensemble. Such pH-driven conformational equilibria could regulate the expression of virulence genes as observed in experiments.²³ In this work, we explore the pH-sensitivity of Cnu and a mutant H45V through multiple equilibrium spectroscopic assays highlighting the presence of a pH-driven conformational switch or population redistribution within the native ensemble. Tryptophan QY and lifetime measurements, local and highly sensitive probes of structure, reveal pH-dependent nonlocal and non-native interactions involving the fourth helix that could be crucial for function. In parallel, we employ the Ising-like statistical mechanical Wako–Saitô–Muñoz–Eaton (WSME) model^{40,41} to reproduce some of the basic experimental observations on Cnu while simultaneously predicting conformational characteristics that could be tested further by experiments or simulations.

MATERIALS AND METHODS

Protein Purification and Spectroscopic Experiments.

The protocols for protein purification and the majority of the spectroscopic experiments can be found in references 18 and 19. The buffers used in the pH-dependent study were glycine-HCl (pH 2–3), sodium acetate (pH 3.5–5.5), and sodium

phosphate (pH 6–8). The ionic strength of sodium phosphate buffer was corrected to 170 mM with NaCl as before. The protein showed signs of irreversibility at higher ionic strengths in low pH buffer necessitating the use of 20 mM ionic strength conditions. Cnu exhibits just ~3 K lower T_m at 20 mM ionic strength conditions at pH 8 compared to 170 mM, and hence, this does not affect the overall conclusions presented in this work.

Electrostatic Potential Calculations. The electrostatic potential maps of Cnu were calculated at experimental conditions (170 mM ionic strength at pH 8 and 20 mM ionic strength at pH 5, 298 K) using the adaptive Poisson–Boltzmann solver (APBS) plugin in PyMOL.⁴² The input PQR files were generated by PDB2PQR server using the Amber force-field and the protonation states were assigned by PROPKA. The grid dimensions were automatically set by the APBS plugin according to the dimensions of input Cnu structure. The electrostatic potentials were calculated by solving the nonlinear Poisson–Boltzmann equation with a single DH sphere boundary condition. The solvent accessible surface area was calculated using a solvent radius of 1.4 Å.

Size-Exclusion Chromatography. The Stokes radii of Cnu and H45V in 170 mM ionic strength conditions were determined by size-exclusion chromatography using a GE HiLoad 26/600 Superdex 75pg column. The column was calibrated with four different proteins with known Stokes radii: Aprotinin (13.5 Å), cytochrome C (17.7 Å), carbonic anhydrase (23.5 Å), and bovine serum albumin (34.8 Å). NaCl and blue dextran 2000 (2 MDa) were used to determine the total and void volumes of the column, respectively.

Fluorescence Lifetime Measurements. Tryptophan lifetime measurements were carried out in a time-domain fluorimeter (ChronosBH, ISS Inc.) with picosecond resolution. Sample temperature (278–363 K) was controlled by a Peltier unit (Quantum Northwest Inc.) coupled to the cuvette holder. A 300 nm LED was used as an excitation source for selective excitation of tryptophan. The excitation beam was passed through a UV grade Glan-Thompson polarizer set at 0° to allow passage of vertically polarized light. The emitted light was passed through another UV grade Glan-Thompson polarizer set at the magic angle (54.7°), with respect to excitation, to avoid polarization effects on the measured lifetime. A 345 nm long-pass filter (SCHOTT) was placed between the sample and detector to reduce scattering artifacts, while Ludox solution was employed for measuring the instrument response function (IRF). All decay curves were recorded until either the peak count reached 10⁴ or the total count approached 10⁸. The intensity decay traces were fit to biexponential functions (single-exponential fits were consistently poor), and the quality of fits was determined from chi-square values. The mean chi-square value was ~1.25 with an average standard deviation of 0.15.

Wako–Saitô–Muñoz–Eaton (WSME) Model. The WSME model is a structure-based and Ising-like statistical mechanical model that employs a binary description for the conformational status of residues.^{40,41} The conformational status of every residue can be 1 (for folded-like, Fol) or 0 (for unfolded-like, Unf) resulting in an ensemble of 2^N microstates for an *N*-residue protein. An entropic penalty (ΔS_{conf}) is therefore invoked to fix every residue in the native conformation given that $\Omega_{\text{Unf}}/\Omega_{\text{Fol}} \gg 1$, where Ω represents the multiplicity of states. Multiple versions of the model are

currently available differing both in the way the ensemble is constructed and the details of the energy function.^{43–53}

In the current work, we employ the exact-solution approach of Wako and Saitô,⁴⁰ and later pioneered independently by Muñoz and Eaton,⁴¹ with the assumption that for any two residues to interact all of the intervening residues should be folded. The current model version is also supplemented with multiple terms, packing from van der Waals interactions (E_{vdW}), native electrostatics modeled by the Debye–Hückel theory (E_{elec}), simplified solvation (ΔG_{solv}), and excess conformational entropy ($\Delta\Delta S_{\text{conf}}$).^{50,52} Briefly, the free energy of each microstate defined by a string of 1s between and including m and n is given by

$$\Delta F_{m,n} = \sum \Delta G_{m,n}^{\text{stab}} - T \sum_m^n \Delta S \quad (1)$$

where

$$\Delta G_{m,n}^{\text{stab}} = E_{\text{vdW}} + E_{\text{elec}} + \Delta G_{\text{solv}} \quad (2)$$

In eq 1, $\Delta S = \Delta S_{\text{conf}}$ if the residue is identified to be structured in the PDB file (say, helix or strand) or $\Delta S = \Delta S_{\text{conf}} + \Delta\Delta S_{\text{conf}}$ if the residue is disordered (coil). We have employed the transfer-matrix formalism of Wako and Saitô to calculate the total partition function, partial partition functions, and residue probabilities.⁴⁰ The parameters are listed in the Table T1.

RESULTS AND DISCUSSION

Natural pH-Switch in Cnu. The far-UV CD monitored unfolding curve of Cnu displays a sigmoidal transition, a flat pretransition region, and an apparent melting temperature (T_m , from a first derivative analysis) of ~ 333 K (Figure 1C). The unfolding curves as a function of pH exhibit nontrivial pretransition slopes and signal magnitudes, indicating complex structural changes (Figure S1A). The melting temperature, on the other hand, displays a clear trend with pH; the T_m changes sharply in two distinct pH regimes with apparent pK_a values of ~ 5.1 and ~ 2.9 , respectively (Figure 2A). The macroscopic pK_a of 2.9 arises from the protonation of acidic side-chains and is a superimposition of multiple microscopic pK_a values of the different aspartates and glutamates. The higher pK_a of 5.1 arises likely from the protonation of H45 that is partially buried in the structure of Cnu. To verify this and to rule out potential stability changes from the protonation of H25 and H68, we generated the mutant H45V; the mutant displays an identical T_m as that of the WT but a slightly steeper pretransition (Figure 1C). Interestingly, the single mutation completely eliminates the pH-driven complex structural changes in the pretransition, as observed in the WT (Figure S1B). Moreover, only a single sharp pH dependent T_m change is observed with an apparent pK_a of 2.9 (Figure 2B).

The observations above validate our hypothesis that a pH-sensing feature, apart from a thermosensor-like property,¹⁸ is embedded in the structure of Cnu through the partially buried histidine. However, electrostatic calculations (Figure 1B) highlight that the protonation generates large electrostatic frustration in the neighborhood of H45, which would effectively disrupt the structure at least in its vicinity. Far-UV CD unfolding curves show little evidence for this expectation, except for a small difference in the pretransition slopes at pH 8, raising questions on whether electrostatic calculations overestimate the extent of unfavorable interactions. Experiments

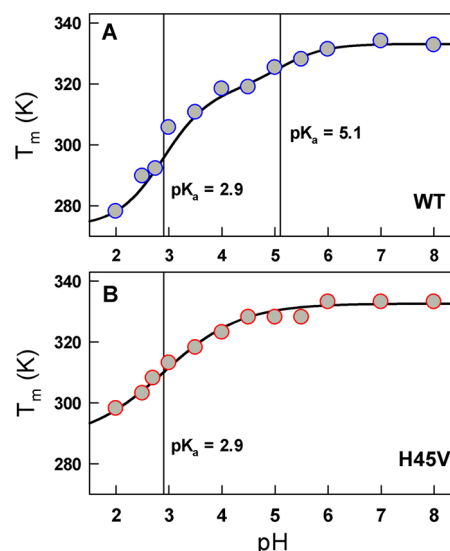


Figure 2. Stability changes of WT Cnu (panel A) and the mutant H45V (panel B) on pH modulations. The vertical dashed lines indicate the apparent pK_a values estimated from a fit to the Henderson–Hasselbalch equation (black curves).

have however shown that changes in the pretransition of equilibrium unfolding curves can be indicative of dramatic changes in the folding mechanism and conformational behavior.^{54–56} In this regard, it has been established that the fourth helix of Cnu and the loop that connects the third and fourth helices (that abuts H45) display large fluctuations in equilibrium; the fourth helix thus accesses partially disordered states (labeled N^*) over a broad free energy well in the native side of the main unfolding barrier.^{18,19} It is therefore possible that the protonated Cnu (at $pH \sim 5$) and the mutant H45V (at $pH 8$) exhibit an altered equilibrium in which the fourth helix is either partially structured or even disordered compared to the WT.

Nontrivial Structural Perturbations. We performed a series of spectroscopic experiments on the WT and the mutant H45V to probe for structural changes (if any) and their features that are invisible to far-UV CD. The tertiary structure of WT Cnu undergoes complex rearrangements between pH 8 and pH 5, which is different from the structural changes observed in the mutant (near-UV CD; Figure 3A,B). Interestingly, the mutant near-UV CD spectrum at pH 8 is different from the WT at the same pH in terms of the overall amplitude of the finer structural features. The quantum yields at 295 nm (W_{67} in the fourth helix; QY_{295}) or at 274 nm (QY_{274}) are also markedly different with distinct amplitudes and temperature dependencies between the WT and the mutant at equivalent pH values (Figure S2). The QY_{295} decreases sharply with the pH exhibiting an apparent pK_a of 5.4, while little change is observed in H45V corroborating the far-UV CD experiments (Figure 3C).

The experiments above indicate that protonation or the H45V mutation induces structural changes in the fourth helix and adjoining regions exactly as observed in temperature- or urea-induced perturbations. Such generic destabilization should, in turn, enhance the population of N^* (a structural ensemble in which the fourth helix is partially disordered) compared to the native state N in which the protein is predominantly folded. We had earlier shown that the proximity of Y40 in the third helix to W67 in the fourth helix serves as a

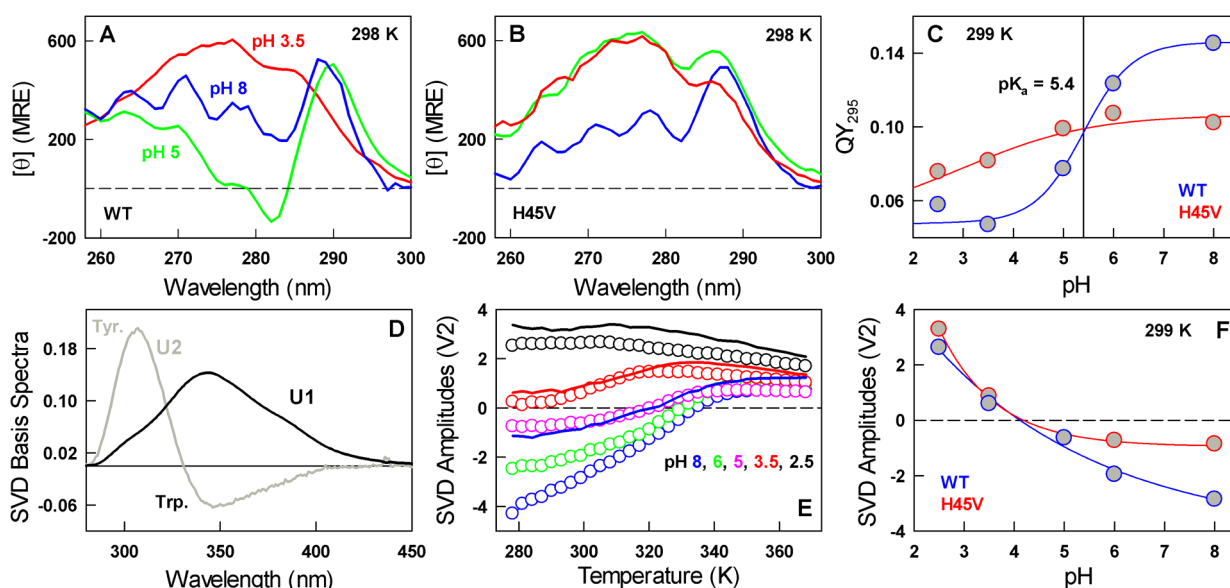


Figure 3. Structural modulations of the native ensemble. (A, B) Near-UV CD spectra of the WT and mutant H45 V at the indicated pH values. (C) Changes in fluorescence quantum yield upon excitation at 295 nm (QY_{295}). The vertical dashed line indicates the apparent pK_a value for the WT. (D) Basis spectra, U1 and U2, from a global singular value decomposition (SVD) analysis of the temperature-wavelength fluorescence emission spectra of both the WT and the mutant upon excitation at 274 nm. The associated singular values account for 81 and 6% of the total basis, respectively. (E) Changes in the amplitude of the second component (V_2) as a function of temperature and pH for the WT (circles) and mutant H45V (curves). The V_2 amplitudes of the mutant at pH 5 and 6 are near identical to pH 8 and hence are not shown for the sake of clarity. (F) Same as in panel E but shown at 299 K as a function of pH. The curves are shown to guide the eye.

natural donor–acceptor FRET (Förster resonance energy transfer) pair.¹⁹ We therefore performed a global SVD (singular value decomposition) of the temperature-wavelength fluorescence emission (upon excitation at 274 nm) of the WT and mutant at different pH values. The first component accounts for the average spectral features and its temperature dependence (Figures 3D and S3). The second component displays an anticorrelation between tyrosine and tryptophan emissions (black in Figure 3D); the amplitude is negative at low temperatures and high pH in the WT, indicating large FRET (enhanced tryptophan emission), and hence smaller distances between Y40 and W67 (Figure 3E,F). On the other hand, the amplitude becomes less negative with increasing temperatures or decreasing pH or even upon mutation, highlighting that Y40 and W67 are separated by larger distances thus decreasing FRET (enhanced tyrosine emission). Interestingly, the amplitude of the second component of the WT at pH 5 matches with the amplitude of the mutant in the pH range of 5–8, illustrating that under these matching conditions, both the WT and the mutant likely sample a similar structural ensemble (Figure 3F). We emphasize here that changes in spectroscopic signatures are observed even at 278 K, where the population of the unfolded state is infinitesimally small to exert any effect on the equilibrium signals.

Modulation of Cnu Conformational Landscape. Given the substantial differences in spectroscopic features upon mutation, we expect the global thermodynamic fluctuations^{57–59} of the mutant to be distinct compared to the WT. To test for this, we measure the absolute heat capacity profiles of Cnu and H45V mutant at pH 8 from the concentration dependence of apparent heat capacities.⁶⁰ The mutant displays larger basal fluctuations ($\sim 20\%$ greater than the WT and relative to the unfolded MP baseline at low temperatures) and a more shallow and broader excess heat capacity curve compared to the WT (Figure 4A). The large basal fluctuation

is evidence that the mutant samples additional conformational substates. If a part of Cnu is more unstructured, it is expected to increase the molecule dimensions proportionately. True to this, size-exclusion chromatography at 298 K reveals that the mutant elutes earlier and with a more skewed elution profile (inset to Figure 4A). The apparent Stokes radius, R_s , of H45V is estimated to be 17.9 Å, compared to an R_s of 17.2 Å for WT, corresponding to a $\sim 14\%$ increase in molecular volume. To extract more information, we quantify the thermograms employing the WSME model that includes multiple energy terms apart from structure-based excess conformational entropy (see the Materials and Methods section). The model fits the data very well, resulting in a native ensemble that can be coarsely partitioned into two macrostates, N and N*; the WT and mutant display distinguishable population distributions even at 298 K (Figure 4B,C). N* is characterized by an enhanced disorder in the fourth helix where W67 is located (Figure 4D).

The heat capacity profile of the WT at pH 5 displays baseline features similar to that of the mutant with enhanced structural fluctuations (pink in Figure 4E). The melting temperature and the overall unfolding enthalpy are substantially lower than the WT, indicating loss of stabilizing interactions. As a first step toward understanding the conformational implications, we analyzed the thermogram with the WSME model in which H45 is either deprotonated (His^0) or protonated (His^+ ; light and dark green curves in Figure 4E). The model predicts substantial loss of order in the fourth helix with the protonation contributing to additional structural changes in regions involving the first helix. The one-dimensional free energy profiles point to an enhanced population of N* but with an additional intermediate-like conformation being populated on protonation (green in Figure 4F). It is important to note that at pH 5, both the protonation states of histidine are equally possible (as the pK_a is ~ 5.1), and

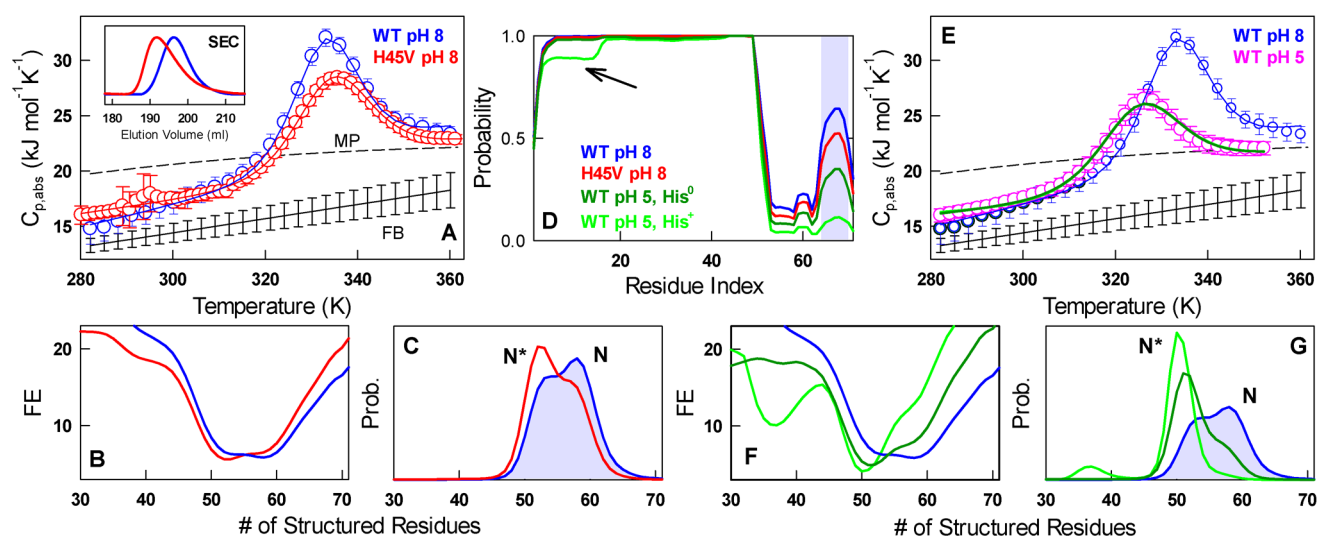


Figure 4. Thermodynamic fluctuations and the conformational landscape of Cnu. (A) The absolute heat capacity profiles (circles) together with the fits from the WSME model (curves). FB and MP stand for the Freire⁶¹ (folded) and Makhatadze–Privalov⁶² (MP; unfolded) baselines, respectively. (Inset) Size-exclusion chromatography elution profiles at pH 8, 298 K. (B, C) Free energy profiles (in kJ mol^{-1}) and the corresponding probability densities at 298 K following the color code in panel A. As the unfolded population is near zero under these conditions, only the folded-like ensembles are shown for the sake of clarity. (D) Folded probability as a function of residue index at 298 K. The arrow highlights minor changes in the structure corresponding to residues in the first helix, while the shaded region marks the fourth helix. (E) The absolute heat capacity profiles (circles) and fits from the WSME model (curves). The light and dark green curves from fits to the WSME model, following the color code from panel D, are superimposable. (F, G) Free energy profiles and the corresponding probability densities at 298 K following the color code in panel D.

hence the native conformational ensemble of Cnu is expected to be an effective combination of the free energy profiles shown in green (Figure 4E,G). A *denovo* prediction of the pH 5 DSC profile (by protonating H45 and using the WT pH 8 parameters) results in similar population redistribution within the native ensemble (Figure S4), attesting to the robustness of the predictions.

Distinct Conformations Sampled by the Fourth Helix upon Protonation and Mutation. Temperature-dependent experiments on the WT show that multiple states associated with the fourth helix are long-lived and structured with distinct NMR resonances. Direct experimental evidence for this from NMR experiments is challenging as even the WT ^1H – ^{15}N spectra are characterized by clustered resonances indicative of multiple conformations in slow exchange;¹⁸ these conformations do not just correspond to the fourth helix but to nearly the entire structure. As an alternative, we probe for the extent of structural heterogeneity in the fourth helix of both the WT and mutant by characterizing the number of tryptophan lifetimes (τ) and their amplitudes as a function of temperature and pH (Figure S5). Any differences in either one or both of the lifetime/amplitude are indicative of differences in the sampled conformational ensembles, as the indole ring is very sensitive to the structural environment.^{63,64} As a reference for local structural environment, we also study a disordered peptide (C-pep) derived from the fourth helix harboring the tryptophan.

The W67 in Cnu WT has two distinct lifetimes of ~ 1 and ~ 5 ns with amplitudes of 0.2 and 0.8, respectively, at 298 K and pH 8. The two lifetimes potentially reflect the unfolded-like and folded-like subpopulations as seen by W67. The amplitude of the shorter lifetime increases with temperature, indicating that it should arise from a structural environment in which W67 is more disordered. The amplitudes crossover at ~ 328 K, much lower than the T_m estimate of 334 K from far-

UV CD and DSC. The fact that even the magnitude of the longer lifetime (from folded conformations) is not constant with temperature indicates that the native ensemble is continuously changing in agreement with the graded structural polymorphism within the native ensemble.¹⁸ Interestingly, the tryptophan in C-pep exhibits lifetimes, amplitudes, and crossover temperatures (~ 310 K) very distinct from that of the WT under the same pH 8 conditions. This observation illustrates that the differences between the two are a consequence of nonlocal contacts made by the fourth helix as C-pep accounts for all the local effects.

On changing the pH to 5, the lifetime of W67 in the WT remains the same as that of pH 8, while the amplitude approaches that of C-pep with a crossover temperature of ~ 315 K, much lower than the T_m at pH 5 from far-UV CD (325 K). For the H45V mutant, the amplitudes are near identical at both the pH conditions and comparable to that of the C-pep, but they display distinct lifetimes at pH 8 and pH 5. In other words, the WT Cnu samples very similar conformational substates between pH 8 and 5 (identical lifetimes) with only the relative population modulated (distinct amplitudes). On the other hand, the H45V mutant samples distinct conformational ensembles at the two pH conditions (distinct lifetimes) with the overall population being disordered-like (amplitudes matching the C-pep). This observation provides direct evidence that lowering pH promotes non-native interactions in the regions adjoining W67 in the H45V mutant.

The availability of amplitude information affords a unique opportunity to explore the landscape microstructure, i.e., the regions of the landscape that are probed by W67, as local probes are expected to provide more sensitive information.⁶⁵ We attempt to quantify the differences in the conformational behavior of just the WT and H45V at pH 8, since the pH effects are nontrivial. The presence of two lifetimes reveals that W67 is sensitive to two subensembles, one in which the

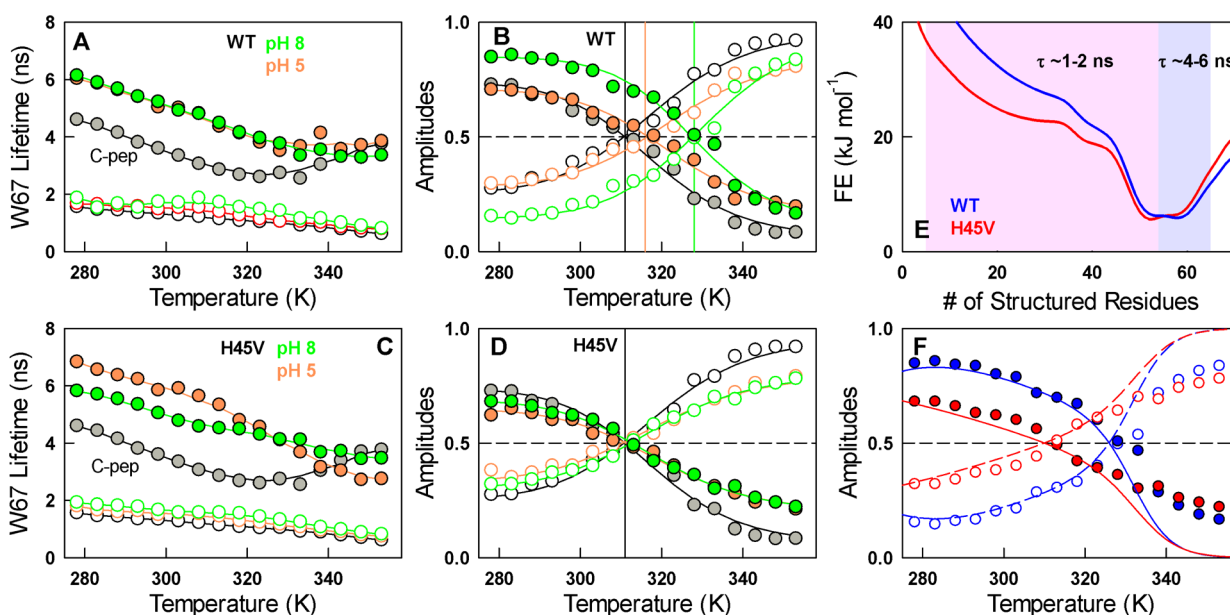


Figure 5. Cnu landscape microstructure from lifetime measurements. (A) Longer (filled circles) and shorter (open circles) W67 lifetimes of the WT at pH 8 (green) and pH 5 (orange). C-pep stands for the 18-residue peptide derived from the fourth helix that acts a reference for local structure that again displays a longer (filled gray) and a shorter (open black) lifetime. The curves are shown to guide the eye. (B) The amplitudes following the color code in panel A for the WT. The vertical lines signal the temperature at which the amplitude reaches 0.5. The curves are shown to guide the eye. Note that the WT displays near-identical lifetimes but differing amplitudes at the two pH conditions explored. (C, D) Lifetime and amplitudes for the H45 V mutant following the pH color code in panels A and B. Note that the mutant displays distinct longer lifetimes but very similar amplitudes at the two pH conditions. (E) One-dimensional free energy profiles at 298 K, pH 8. The blue and pink shaded areas represent the likely partitioning of the folded-like and unfolded-like conformational states as monitored by W67, respectively. (F) Integrated populations from the shaded areas in panel E (curves) for the WT (blue) and mutant (red). The filled and open circles correspond to the respective amplitudes of the longer and shorter lifetimes, respectively.

conformation is disordered-like (shorter lifetime with increasing amplitude with temperature), and another in which the conformation is more ordered (longer lifetime with decreasing amplitude). Using this observation, we iteratively partition the free energy profile into two apparent macrostates as seen by W67 and match the integrated population with the fluorescence lifetime amplitudes for each case. The closest agreement is obtained when 52/53–64 structured residues define the folded-like macrostate (with $\tau \sim 5\text{--}6$ ns), while 4–52/53 structured residues define the unfolded-like macrostate (with $\tau \sim 1\text{--}2$ ns). Such a partitioning is able to simultaneously account for the changes in amplitudes (and hence subpopulations) until the respective inflection points for both the WT and mutant at pH 8. Beyond the apparent melting temperature, the agreement is poor; this is not surprising as the longer lifetime differs across pH and variants at temperatures beyond 330 K (Figure 5A,C).

CONCLUSION

We show here that both mutation and protonation of conserved buried histidine alter the native conformational ensemble of Cnu (N) resulting in a higher fraction of the state N*. This partially structured state is characterized by a larger disorder in the fourth helix. Evidence for this is presented from the perspective of the W67 quantum yield, fluorescence lifetimes and amplitudes, and intramolecular FRET changes. The population redistribution manifests as complex tertiary structural perturbations, enhanced thermodynamic fluctuations, and increased molecular volume of Cnu. It is important to emphasize that the far-UV CD thermal unfolding profiles of the two proteins, WT and H45V, are very similar. However,

when the probe is local (QY) or provides information on distances (FRET) or the second moment of distributions (protein heat capacity), we observe large differences in the conformational behavior that cannot be rationalized by a simple two-state equilibrium between folded and unfolded states. The longer fluorescence lifetime, representative of the folded subpopulation (N), is not constant with the temperature highlighting the presence of continuous structural changes even within this ensemble. Similar changes in the native ensemble have been reported in other proteins indicating that this could be a generic feature of native ensembles.^{18,63,66–68}

The mutant H45V at pH 8 exhibits spectroscopic properties comparable to the Cnu WT at pH 5, particularly from QY and fluorescence lifetime experiments. However, the thermograms are vastly different (Figure 4), indicating that additional regions are also perturbed upon pH modulations. We further show evidence for non-native interactions in the regions adjoining the fourth helix for the mutant at pH 5 through the observation of distinct W67 fluorescence lifetimes. The WSME model predicts nontrivial changes in the free energy landscape of Cnu upon mutation and protonation. Since the model is structure-based, it merely predicts an increased population of N* on mutation but not the finer details of non-native interactions associated with the fourth helix. It should, however, be possible to extract the extent and nature of non-native interactions through atomic-level simulations. The complex structural changes upon a single mutation are also in line with recent experimental–computational evidences that emphasize on the propagation of mutational effects in proteins.^{69,70} Thus, mutational outcomes should be analyzed

with extreme caution as most information is hidden in the average spectroscopic features, and changes are evident only as second-order effects. Finally, our observations point to a unique role for pH in determining the conformational properties of the transcriptional co-repressor Cnu. Since the fourth helix of Cnu is involved in binding with the transcription factor H-NS, the structural redistributions we observe could regulate pathogenic response in enterobacteriaceae in a straightforward manner by modulating the binding affinity.

■ ASSOCIATED CONTENT

Supporting Information

The Supporting Information is available free of charge on the ACS Publications website at DOI: [10.1021/acs.jpccb.8b05108](https://doi.org/10.1021/acs.jpccb.8b05108).

Far-UV CD and fluorescence thermal unfolding curves, amplitudes of the first basis spectra from global SVD of fluorescence emission spectra, fluorescence lifetime decays, and WSME model parameters (PDF)

■ AUTHOR INFORMATION

Corresponding Author

*E-mail: athi@iitm.ac.in; Tel: +91-44-2257 4140.

ORCID

Abhishek Narayan: [0000-0001-5390-2380](https://orcid.org/0000-0001-5390-2380)

Athi N. Naganathan: [0000-0002-1655-7802](https://orcid.org/0000-0002-1655-7802)

Notes

The authors declare no competing financial interest.

■ ACKNOWLEDGMENTS

This work was funded by the Research Support for the Indian National Science Academy (INSA) Young Scientist Medal Award scheme (SP/YSP/132/2016/068) to A.N.N. The spectroscopic instrumentation used in this work was funded by the Wellcome Trust/DBT India Alliance Intermediate Fellowship to A.N.N. (IA/I/15/1/S01837).

■ ABBREVIATIONS

DH, Debye–Hückel; CD, circular dichroism; SEC, size exclusion chromatography; WSME, Wako–Saitō–Muñoz–Eaton; RC, reaction coordinate; DSC, differential scanning calorimetry.

■ REFERENCES

- (1) Hurme, R.; Berndt, K. D.; Namork, E.; Rhen, M. DNA Binding Exerted by a Bacterial Gene Regulator with an Extensive Coiled-Coil Domain. *J. Biol. Chem.* **1996**, *271*, 12626–12631.
- (2) Hurme, R.; Berndt, K. D.; Normark, S. J.; Rhen, M. A Proteinaceous Gene Regulatory Thermometer in Salmonella. *Cell* **1997**, *90*, 55–64.
- (3) Hurme, R.; Rhen, M. Temperature Sensing in Bacterial Gene Regulation—What It All Boils Down To. *Mol. Microbiol.* **1998**, *30*, 1–6.
- (4) Goulian, M. Robust Control in Bacterial Regulatory Circuits. *Curr. Opin. Microbiol.* **2004**, *7*, 198–202.
- (5) Marianayagam, N. J.; Sunde, M.; Matthews, J. M. The Power of Two: Protein Dimerization in Biology. *Trends Biochem. Sci.* **2004**, *29*, 618–625.
- (6) Klinkert, B.; Narberhaus, F. Microbial Thermosensors. *Cell. Mol. Life Sci.* **2009**, *66*, 2661–2676.
- (7) Swint-Kruse, L.; Matthews, K. S. Allosteric in the LacI/GalR Family: Variations on a Theme. *Curr. Opin. Microbiol.* **2009**, *12*, 129–137.
- (8) Bohme, K.; Steinmann, R.; Kortmann, J.; Seekircher, S.; Heroven, A. K.; Berger, E.; Pisano, F.; Thiermann, T.; Wolf-Watz, H.; Narberhaus, F.; et al. Concerted Actions of a Thermo-Labile Regulator and a Unique Intergenic RNA Thermosensor Control *Yersinia* Virulence. *PLoS Pathog.* **2012**, *8*, e1002518.
- (9) Motlagh, H. N.; Li, J.; Thompson, E. B.; Hilser, V. J. Interplay between Allosteric and Intrinsic Disorder in an Ensemble. *Biochem. Soc. Trans.* **2012**, *40*, 975–980.
- (10) Steinmann, R.; Dersch, P. Thermosensing to Adjust Bacterial Virulence in a Fluctuating Environment. *Future Microbiol.* **2013**, *8*, 85–105.
- (11) Atlung, T.; Ingmer, H. H-Ns: A Modulator of Environmentally Regulated Gene Expression. *Mol. Microbiol.* **1997**, *24*, 7–17.
- (12) Garcia, J.; Cordeiro, T. N.; Nieto, J. M.; Pons, I.; Juarez, A.; Pons, M. Interaction between the Bacterial Nucleoid Associated Proteins Hha and H-NS Involves a Conformational Change of Hha. *Biochem. J.* **2005**, *388*, 755–762.
- (13) Stoebel, D. M.; Free, A.; Dorman, C. J. Anti-Silencing: Overcoming H-NS-Mediated Repression of Transcription in Gram-Negative Enteric Bacteria. *Microbiology* **2008**, *154*, 2533–2545.
- (14) de Alba, C. F.; Solorzano, C.; Paytubi, S.; Madrid, C.; Juarez, A.; Garcia, J.; Pons, M. Essential Residues in the H-NS Binding Site of Hha, a Co-Regulator of Horizontally Acquired Genes in Enterobacteria. *FEBS Lett.* **2011**, *585*, 1765–1770.
- (15) Cordeiro, T. N.; Garcia, J.; Bernado, P.; Millet, O.; Pons, M. A Three-Protein Charge Zipper Stabilizes a Complex Modulating Bacterial Gene Silencing. *J. Biol. Chem.* **2015**, *290*, 21200–21212.
- (16) Nieto, J. M.; Madrid, C.; Prenafeta, A.; Miquel, E.; Balsalobre, C.; Carrascal, M.; Juarez, A. Expression of the Hemolysin Operon in *Escherichia Coli* Is Modulated by a Nucleoid-Protein Complex That Includes the Proteins Hha and H-NS. *Mol. Gen. Genet.* **2000**, *263*, 349–358.
- (17) Madrid, C.; Nieto, J. M.; Juarez, A. Role of the Hha/YmoA Family of Proteins in the Thermoregulation of the Expression of Virulence Factors. *Int. J. Med. Microbiol.* **2001**, *291*, 425–432.
- (18) Narayan, A.; Campos, L. A.; Bhatia, S.; Fushman, D.; Naganathan, A. N. Graded Structural Polymorphism in a Bacterial Thermosensor Protein. *J. Am. Chem. Soc.* **2017**, *139*, 792–802.
- (19) Narayan, A.; Naganathan, A. N. Tuning the Continuum of Structural States in the Native Ensemble of a Regulatory Protein. *J. Phys. Chem. Lett.* **2017**, *8*, 1683–1687.
- (20) Slonczewski, J. L.; Fujisawa, M.; Dopson, M.; Krulwich, T. A. Cytoplasmic pH Measurement and Homeostasis in Bacteria and Archaea. *Adv. Microb. Physiol.* **2009**, *55*, 1.
- (21) Krulwich, T. A.; Sachs, G.; Padan, E. Molecular Aspects of Bacterial pH Sensing and Homeostasis. *Nat. Rev. Microbiol.* **2011**, *9*, 330–343.
- (22) Lund, P.; Tramonti, A.; De Biase, D. Coping with Low pH: Molecular Strategies in Neutralophilic Bacteria. *FEMS Microbiol. Rev.* **2014**, *38*, 1091–1125.
- (23) Silphaduang, U.; Mascarenhas, M.; Karmali, M.; Coombes, B. K. Repression of Intracellular Virulence Factors in Salmonella by the Hha and YdgT Nucleoid-Associated Proteins. *J. Bacteriol.* **2007**, *189*, 3669–3673.
- (24) Tanford, C. Protein Denaturation. *Adv. Protein Chem.* **1968**, *23*, 121–282.
- (25) Tanford, C.; Roxby, R. Interpretation of Protein Titration Curves. Application to Lysozyme. *Biochemistry* **1972**, *11*, 2192–2198.
- (26) Yang, A. S.; Honig, B. On the pH Dependence of Protein Stability. *J. Mol. Biol.* **1993**, *231*, 459–474.
- (27) Yang, A. S.; Honig, B. Structural Origins of pH and Ionic Strength Effects on Protein Stability. Acid Denaturation of Sperm Whale Apomyoglobin. *J. Mol. Biol.* **1994**, *237*, 602–614.
- (28) Antosiewicz, J.; McCammon, J. A.; Gilson, M. K. Prediction of pH-Dependent Properties of Proteins. *J. Mol. Biol.* **1994**, *238*, 415–436.
- (29) Geierstanger, B.; Jamin, M.; Volkman, B. F.; Baldwin, R. L. Protonation Behavior of Histidine 24 and Histidine 119 in Forming

the pH 4 Folding Intermediate of Apomyoglobin. *Biochemistry* **1998**, *37*, 4254–4265.

(30) Onufriev, A.; Case, D. A.; Ullmann, G. M. A Novel View of pH Titration in Biomolecules. *Biochemistry* **2001**, *40*, 3413–3419.

(31) Jamin, M.; Geierstanger, B.; Baldwin, R. L. The pKa of His-24 in the Folding Transition State of Apomyoglobin. *Proc. Natl. Acad. Sci. U. S. A.* **2001**, *98*, 6127–6131.

(32) Fitch, C. A.; Whitten, S. T.; Hilser, V. J.; Garcia-Moreno, E. B. Molecular Mechanisms of pH-Driven Conformational Transitions of Proteins: Insights from Continuum Electrostatics Calculations of Acid Unfolding. *Proteins: Struct., Funct., Genet.* **2006**, *63*, 113–126.

(33) Keeler, C.; Tettamanzi, M. C.; Meshack, S.; Hodsdon, M. E. Contribution of Individual Histidines to the Global Stability of Human Prolactin. *Protein Sci.* **2009**, *18*, 909–920.

(34) Shi, C.; Wallace, J. A.; Shen, J. K. Thermodynamic Coupling of Protonation and Conformational Equilibria in Proteins: Theory and Simulation. *Biophys. J.* **2012**, *102*, 1590–1597.

(35) Chimentì, M. S.; Khangulov, V. S.; Robinson, A. C.; Heroux, A.; Majumdar, A.; Schlessman, J. L.; Garcia-Moreno, B. Structural Reorganization Triggered by Charging of Lys Residues in the Hydrophobic Interior of a Protein. *Structure* **2012**, *20*, 1071–1085.

(36) Schonichen, A.; Webb, B. A.; Jacobson, M. P.; Barber, D. L. Considering Protonation as a Posttranslational Modification Regulating Protein Structure and Function. *Annu. Rev. Biophys.* **2013**, *42*, 289–314.

(37) Di Russo, N. V.; Marti, M. A.; Roitberg, A. E. Underlying Thermodynamics of pH-Dependent Allostery. *J. Phys. Chem. B* **2014**, *118*, 12818–12826.

(38) Watanabe, S.; Harayama, M.; Kanemura, S.; Sitia, R.; Inaba, K. Structural Basis of pH-Dependent Client Binding by Erp44, a Key Regulator of Protein Secretion at the ER-Golgi Interface. *Proc. Natl. Acad. Sci. U. S. A.* **2017**, *114*, E3224–e3232.

(39) Liu, J.; Swails, J.; Zhang, J. Z. H.; He, X.; Roitberg, A. E. A Coupled Ionization-Conformational Equilibrium Is Required to Understand the Properties of Ionizable Residues in the Hydrophobic Interior of Staphylococcal Nuclease. *J. Am. Chem. Soc.* **2018**, *140*, 1639–1648.

(40) Wako, H.; Saito, N. Statistical Mechanical Theory of Protein Conformation 0.2. Folding Pathway for Protein. *J. Phys. Soc. Jpn.* **1978**, *44*, 1939–1945.

(41) Muñoz, V.; Eaton, W. A. A Simple Model for Calculating the Kinetics of Protein Folding from Three-Dimensional Structures. *Proc. Natl. Acad. Sci. U. S. A.* **1999**, *96*, 11311–11316.

(42) Jurrus, E.; Engel, D.; Star, K.; Monson, K.; Brandi, J.; Felberg, L. E.; Brookes, D. H.; Wilson, L.; Chen, J.; Liles, K.; et al. Improvements to the APBS Biomolecular Solvation Software Suite. *Protein Sci.* **2018**, *27*, 112–128.

(43) Henry, E. R.; Eaton, W. A. Combinatorial Modeling of Protein Folding Kinetics: Free Energy Profiles and Rates. *Chem. Phys.* **2004**, *307*, 163–185.

(44) Imparato, A.; Pelizzola, A.; Zamparo, M. Ising-Like Model for Protein Mechanical Unfolding. *Phys. Rev. Lett.* **2007**, *98*, 148102.

(45) Kubelka, J.; Henry, E. R.; Cellmer, T.; Hofrichter, J.; Eaton, W. A. Chemical, Physical, and Theoretical Kinetics of an Ultrafast Folding Protein. *Proc. Natl. Acad. Sci. U. S. A.* **2008**, *105*, 18655–18662.

(46) Henry, E. R.; Best, R. B.; Eaton, W. A. Comparing a Simple Theoretical Model for Protein Folding with All-Atom Molecular Dynamics Simulations. *Proc. Natl. Acad. Sci. U. S. A.* **2013**, *110*, 17880–17885.

(47) Godoy-Ruiz, R.; Henry, E. R.; Kubelka, J.; Hofrichter, J.; Muñoz, V.; Sanchez-Ruiz, J. M.; Eaton, W. A. Estimating Free-Energy Barrier Heights for an Ultrafast Folding Protein from Calorimetric and Kinetic Data. *J. Phys. Chem. B* **2008**, *112*, 5938–5949.

(48) Inanami, T.; Terada, T. P.; Sasai, M. Folding Pathway of a Multidomain Protein Depends on Its Topology of Domain Connectivity. *Proc. Natl. Acad. Sci. U. S. A.* **2014**, *111*, 15969–15974.

(49) Bruscolini, P.; Naganathan, A. N. Quantitative Prediction of Protein Folding Behaviors from a Simple Statistical Model. *J. Am. Chem. Soc.* **2011**, *133*, 5372–5379.

(50) Naganathan, A. N. Predictions from an Ising-Like Statistical Mechanical Model on the Dynamic and Thermodynamic Effects of Protein Surface Electrostatics. *J. Chem. Theory Comput.* **2012**, *8*, 4646–4656.

(51) Caraglio, M.; Pelizzola, A. Effects of Confinement on Thermal Stability and Folding Kinetics in a Simple Ising-Like Model. *Phys. Biol.* **2012**, *9*, 016006.

(52) Rajasekaran, N.; Gopi, S.; Narayan, A.; Naganathan, A. N. Quantifying Protein Disorder through Measures of Excess Conformational Entropy. *J. Phys. Chem. B* **2016**, *120*, 4341–4350.

(53) Gopi, S.; Singh, A.; Suresh, S.; Paul, S.; Ranu, S.; Naganathan, A. N. Toward a Quantitative Description of Microscopic Pathway Heterogeneity in Protein Folding. *Phys. Chem. Chem. Phys.* **2017**, *19*, 20891–20903.

(54) Garcia-Mira, M. M.; Sadqi, M.; Fischer, N.; Sanchez-Ruiz, J. M.; Muñoz, V. Experimental Identification of Downhill Protein Folding. *Science* **2002**, *298*, 2191–2195.

(55) Liu, F.; Gruebele, M. Tuning Lambda(6–85) Towards Downhill Folding at Its Melting Temperature. *J. Mol. Biol.* **2007**, *370*, 574–584.

(56) Naganathan, A. N.; Li, P.; Perez-Jimenez, R.; Sanchez-Ruiz, J. M.; Muñoz, V. Navigating the Downhill Protein Folding Regime Via Structural Homologues. *J. Am. Chem. Soc.* **2010**, *132*, 11183–11190.

(57) Cooper, A. Thermodynamic Fluctuations in Protein Molecules. *Proc. Natl. Acad. Sci. U. S. A.* **1976**, *73*, 2740–2741.

(58) Sanchez-Ruiz, J. M. Probing Free-Energy Surfaces with Differential Scanning Calorimetry. *Annu. Rev. Phys. Chem.* **2011**, *62*, 231–255.

(59) Ibarra-Molero, B.; Naganathan, A. N.; Sanchez-Ruiz, J. M.; Muñoz, V. Modern Analysis of Protein Folding by Differential Scanning Calorimetry. *Methods Enzymol.* **2016**, *567*, 281–318.

(60) Guzman-Casado, M.; Parody-Morreale, A.; Robic, S.; Marqusee, S.; Sanchez-Ruiz, J. M. Energetic Evidence for Formation of a pH-Dependent Hydrophobic Cluster in the Denatured State of *Thermus thermophilus* Ribonuclease H. *J. Mol. Biol.* **2003**, *329*, 731–743.

(61) Gomez, J.; Hilser, V. J.; Xie, D.; Freire, E. The Heat-Capacity of Proteins. *Proteins: Struct., Funct., Genet.* **1995**, *22*, 404–412.

(62) Privalov, P. L.; Makhatazde, G. I. Heat Capacity of Proteins. II. Partial Molar Heat Capacity of the Unfolded Polypeptide Chain of Proteins: Protein Unfolding Effects. *J. Mol. Biol.* **1990**, *213*, 385–391.

(63) Lakshmikanth, G. S.; Sridevi, K.; Krishnamoorthy, G.; Udgaonkar, J. B. Structure Is Lost Incrementally During the Unfolding of Barstar. *Nat. Struct. Biol.* **2001**, *8*, 799–804.

(64) Jha, S. K.; Dhar, D.; Krishnamoorthy, G.; Udgaonkar, J. B. Continuous Dissolution of Structure During the Unfolding of a Small Protein. *Proc. Natl. Acad. Sci. U. S. A.* **2009**, *106*, 11113–11118.

(65) Sukenik, S.; Pogorelov, T. V.; Gruebele, M. Can Local Probes Go Global? A Joint Experiment-Simulation Analysis of Lambda(6–85) Folding. *J. Phys. Chem. Lett.* **2016**, *7*, 1960–1965.

(66) Campos, L. A.; Sadqi, M.; Liu, J. W.; Wang, X.; English, D. S.; Muñoz, V. Gradual Disordering of the Native State on a Slow Two-State Folding Protein Monitored by Single-Molecule Fluorescence Spectroscopy and Nmr. *J. Phys. Chem. B* **2013**, *117*, 13120–13131.

(67) Law, A. B.; Sapienza, P. J.; Zhang, J.; Zuo, X.; Petit, C. M. Native State Volume Fluctuations in Proteins as a Mechanism for Dynamic Allostery. *J. Am. Chem. Soc.* **2017**, *139* (10), 3599.

(68) Bhatia, S.; Krishnamoorthy, G.; Udgaonkar, J. B. Site-Specific Time-Resolved FRET Reveals Local Variations in the Unfolding Mechanism in an Apparently Two-State Protein Unfolding Transition. *Phys. Chem. Chem. Phys.* **2018**, *20*, 3216–3232.

(69) Rajasekaran, N.; Suresh, S.; Gopi, S.; Raman, K.; Naganathan, A. N. A General Mechanism for the Propagation of Mutational Effects in Proteins. *Biochemistry* **2017**, *56*, 294–305.

(70) Rajasekaran, N.; Sekhar, A.; Naganathan, A. N. A Universal Pattern in the Percolation and Dissipation of Protein Structural Perturbations. *J. Phys. Chem. Lett.* **2017**, *8*, 4779–4784.